



A Journal of



Accepted Article

Title: Monocationic Iridium(III) Complexes with Far-Red Charge Transfer Absorption and Near-IR Emission: Synthesis, Photophysics, and Reverse Saturable Absorption

Authors: Bingqing Liu, Levi Lystrom, Colin G. Cameron, Svetlana Kilina, Sherri A. McFarland, and Wenfang Sun

This manuscript has been accepted after peer review and appears as an Accepted Article online prior to editing, proofing, and formal publication of the final Version of Record (VoR). This work is currently citable by using the Digital Object Identifier (DOI) given below. The VoR will be published online in Early View as soon as possible and may be different to this Accepted Article as a result of editing. Readers should obtain the VoR from the journal website shown below when it is published to ensure accuracy of information. The authors are responsible for the content of this Accepted Article.

To be cited as: *Eur. J. Inorg. Chem.* 10.1002/ejic.201900156

Link to VoR: <http://dx.doi.org/10.1002/ejic.201900156>

WILEY-VCH

FULL PAPER

Monocationic Iridium(III) Complexes with Far-Red Charge Transfer Absorption and Near-IR Emission: Synthesis, Photophysics, and Reverse Saturable Absorption

Bingqing Liu,^[a] Levi Lystrom,^[a] Colin G. Cameron,^[b] Svetlana Kilina,^[a] Sherri A. McFarland,^[b] and Wenfang Sun^{*[a]}

Abstract: The synthesis, photophysics, and reverse saturable absorption (RSA) of three monocationic iridium(III) complexes (**Ir1**–**Ir3**) bearing diimine (N[^]N) ligand with different degrees of π -conjugation are reported. Spectroscopic methods, including UV-vis absorption, emission, and transient absorption spectroscopy, and density functional theory calculations were carried out to understand the nature of the singlet and triplet optical transitions and the influence of N[^]N ligand π -conjugation on the photophysical properties of the complexes. All complexes possessed predominant ligand-centered $^1\pi,\pi^*$ absorption bands at 280–420 nm and weak charge-transfer absorption bands at 420–610 nm for **Ir1**, 420–680 nm for **Ir2**, and 420–730 nm for **Ir3**. The extended π -conjugation of the N[^]N ligand red-shifted the charge transfer absorption bands and increased the molar extinction coefficients of all of the absorption bands. All complexes were emissive in the far-red to the near-infrared regions, with the emission energies gradually decreasing when the π -conjugation of the N[^]N ligand increased. However, the emission lifetime of **Ir3** increased when its emitting state energy decreased. This was caused by the different nature of the T₁ state in **Ir3**, which was the predominant N[^]N ligand-localized $^3\pi,\pi^*$ state, compared to the charge transfer T₁ states in **Ir1** and **Ir2**. The different parentages of the T₁ state in **Ir3** also gave rise to a much broader and stronger triplet excited-state absorption in the 420–800 nm regions. The varied ground-state and triplet excited-state absorption characteristics led to a different strength of the reverse saturable absorption (RSA) for ns laser pulses at 532 nm, with the RSA strength following the trend of **Ir3** > **Ir1** ≥ **Ir2**. Complex **Ir3** is particularly attractive for its potential as a broadband reverse saturable absorber in view of its broader ground- and excited-state absorption in the regions of 420–730 nm and longer-lived triplet excited state.

Introduction

In the past two decades, octahedral d⁶ Ir(III) complexes have attracted an intense interest among chemists and materials scientists because of their high triplet excited-state quantum yields, synthetic versatility, and chemical stability.^[1–4] The rich photophysical and electrochemical properties of the Ir(III) complexes prompt their potential applications in phosphorescence-based organic light-emitting diodes,^[5,6]

low-power upconversion,^[7,8] biomolecular labelling and imaging,^[9,10] photochemical water oxidation,^[11,12] photodynamic therapy,^[13–15] and nonlinear optics.^[16,17]

Among the different types of Ir(III) complexes, monocationic Ir(III) complexes featuring diimine (N[^]N) and cyclometalating (C[^]N) ligands are particularly interesting because of the facile synthesis under a mild condition. In addition, the absorption and emission characteristics of this type of complexes can be readily tuned via exploiting different N[^]N and/or C[^]N ligands.^[18–20] Based on the reported electrochemical and computational studies, electrons of the lowest unoccupied molecular orbitals (LUMO) of this type of complexes are typically distributed on the N[^]N ligand, whereas the electrons of the highest occupied molecular orbitals (HOMO) are mainly delocalized on the C[^]N ligands and d-orbital of the metal center.^[21] Therefore, variation of the N[^]N ligand mainly impacts the energy of the LUMO, but has a negligible effect on the energy of the HOMO.^[22] This effect makes it possible to readily tune the lowest-energy charge transfer absorption band corresponding to the HOMO→LUMO transition via alternation of the N[^]N ligand. Meanwhile, the lowest triplet excited states (T₁ states) of the complexes can be altered simultaneously.^[23] For this reason, tremendous efforts have been put on extending the synthetic scope of the N[^]N ligands, with 2,2'-bipyridine (bpy) and its analogy being the most commonly explored ones to date.^[24–26]

Reverse saturable absorption (RSA) is a nonlinear optical phenomenon in which the reverse saturable absorbers exhibit a linear absorption at low incident laser fluence, while their absorptivity increases when the incident fluence increases. RSA occurs when the excited-state absorption of an absorber is stronger than that of the ground state at the corresponding wavelength. Materials exhibiting broadband and strong RSA have potential applications in optical switching,^[27] optical limiting,^[28] laser mode locking,^[29] optical pulse shaping,^[30] spatial light modulation,^[30,31] and laser beam compression,^[32] etc. In order to facilitate RSA of nanosecond laser pulses, an absorber should have a weak ground-state absorption to populate the excited states, but long-lived triplet excited states, large triplet-triplet excited-state absorption coefficients, and a high quantum yield for triplet excited-state formation. In recent years, the RSA of heavy transition-metal complexes, such as octahedral Ir(III) complexes, have been extensively explored by our group^[14,16,17,24,33–42] and other groups^[23,43–45] because these complexes displayed the aforementioned characteristics that well match the requirements for RSA. In

[a] Department of Chemistry and Biochemistry, North Dakota State University, Fargo, North Dakota 58108–6050, United States. E-mail: Wenfang.Sun@ndsu.edu
<https://www.ndsu.edu/chemistry/people/faculty/sun.html>

[b] Department of Chemistry and Biochemistry, University of North Carolina at Greensboro, Greensboro, North Carolina 27402-6170, United States

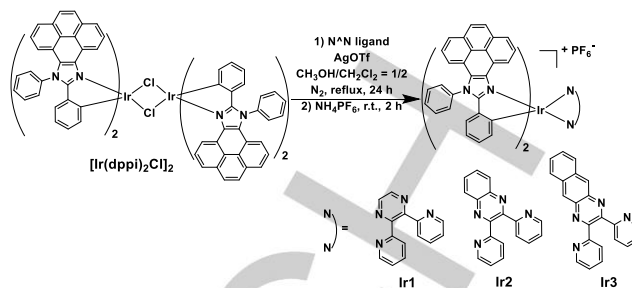
Supporting information for this article is given via a link at the end of the document.

FULL PAPER

addition, by structural modifications, both the ground- and excited-state properties can be readily tuned in these complexes for optimization of the RSA.

Although extensive work has been reported on Ir(III) complexes for RSA, challenges still exist in developing the Ir(III) complexes into broadband reverse saturable absorbers. Among which the lack of considerable ground-state absorption in the red to the near-infrared (NIR) regions remains to be one of the obstacles. In seeking solutions to red-shift the ground-state absorption but meanwhile keep a long-lived and strongly absorbing triplet excited state, immense effects have been put by our group on exploring N[^]N or C[^]N ligands suitable for reverse saturable absorbers.^[14,16,17,24,33–42] We discovered that incorporation of quinoxaline or benzo[*g*]quinoxaline unit into either the N[^]N or C[^]N ligand red-shifted the spin-forbidden ³π,π*/³CT (charge transfer) absorption bands into longer wavelengths.^[14,36,41] However, the triplet excited-state lifetimes of these complexes were reduced to tens to hundreds of nanoseconds (ns). On the other hand, we have reported that Ir(III) bipyridine complex bearing 1,2-diphenyl-9*H*-pyreno[4,5-*d*]imidazole (dppi) cyclometalating ligands displayed a long-lived triplet excited state and strong triplet excited-state absorption in the spectral regions of 410 – 700 nm.^[24]

Inspired by our previous explorations, we combine these two approaches in one system, attempting to red-shift the ground-state absorption to the far-red / NIR regions and meanwhile keep a relatively long-lived and broadly absorbing triplet excited state. Our ultimate goal is to develop broadband reverse saturable absorbers for optical limiting or optical switching applications. To realize this goal, in this work, we synthesized and investigated three cationic Ir(III) complexes featuring dppi C[^]N ligands and pyrazine-based N[^]N ligands (structures shown in Scheme 1) as reverse saturable absorbers. The π-conjugation of the N[^]N ligands are gradually extended from **Ir1** to **Ir3** via benzannulation at the pyrazine unit to red-shift the ³π,π* / ^{1,3}CT absorption bands. The 2,3-di(pyridin-2-yl)pyrazine (dpp) moiety would not only cause the red-shift of the ³π,π*/^{1,3}CT absorption bands but also serve as a bridge to construct a supramolecular system that will be studied in the future. In addition to the spectroscopic studies on the photophysical properties of these complexes, density functional theory (DFT) calculation were performed to provide insight into the natures of the singlet and triplet states of these Ir(III) complexes. RSA of these complexes at 532 nm for ns laser pulses was demonstrated.



Scheme 1. Synthetic route for Ir(III) complexes **Ir1–Ir3**.

Results and Discussion

Electronic absorption

The ground-state absorption spectra of complexes **Ir1–Ir3** were measured in CH₂Cl₂ (Fig. 1), and the corresponding data are compiled in Table 1. Since the observed absorption obeyed the Beer's law in the concentration range of 5×10^{−6} to 1×10^{−4} mol·L^{−1}, we consider that no ground-state aggregation occurs in this concentration range.

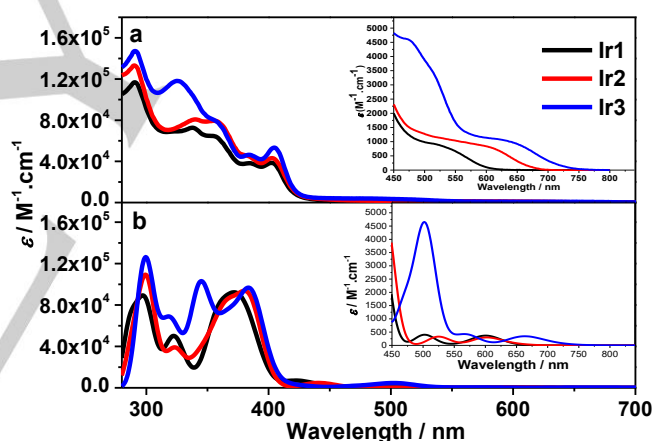


Fig. 1 Experimental (a) and theoretical (b) UV–Vis absorption spectra of **Ir1–Ir3** at room temperature in CH₂Cl₂. The insets show the expanded spectra in the regions of 450 – 800 nm. The B3LYP functional was used in the TDDFT calculations and the calculated transitions were broadened by a Gaussian distribution with a linewidth of 0.08 eV.

The UV–vis absorption spectra of **Ir1–Ir3** resemble each other, being all composed of structured, intense absorption bands in the regions of 280 – 420 nm. The molar extinction coefficients of these bands gradually increased from **Ir1** to **Ir3**, and a new band appearing at 325 nm in **Ir3**. Considering the spectral features and the molar extinction coefficients, we attribute these absorption bands predominantly to the ligand-localized ¹π,π* transitions. The gradually increased molar extinction coefficients are a reflection of the increased transition probability when the π-conjugation of the N[^]N ligand extended. All spectra also exhibited weak and broad tails above 420 nm, i.e. 420 – 610 nm for **Ir1**, 420 – 680 nm for **Ir2**, and 420–730 nm for **Ir3** (see inset in panel (a))

FULL PAPER

of Fig. 1). Because of the structureless feature and small molar extinction coefficients, these band(s) likely arose from charge transfer (CT) transitions. The gradual red-shift of these bands with increased molar extinction coefficients suggested that the CT transitions likely involved the N^N ligands, which could be metal-to-ligand charge transfer (MLCT) and ligand-to-ligand charge transfer (LLCT).

Table 1. Photophysical properties of complexes **Ir1–Ir3**.

	$\lambda_{\text{abs}}/\text{nm}$ ($\log \epsilon$) ^[a]	$\lambda_{\text{em}}/\text{nm}$ ($\tau_{\text{em}}/\text{ns}$); Φ_{em} ^[b]	$\lambda_{\text{T1-Tn}}/\text{nm}$ ($\tau_{\text{T1-Tn}}/\text{ns}$); $\log \epsilon_{\text{T1-Tn}}$; Φ_{T} ^[c]
Ir1	290 (5.06), 338 (4.86), 356 (4.81), 384 (4.58), 402 (4.57), 507 (2.98)	651 (185); 0.036	390 (119; –), 437 (110; 4.41), 702 (108; –); 0.33
Ir2	290 (5.12), 340 (4.91), 355 (4.90), 381 (4.66), 402 (4.63), 544 (3.03)	710 (70); 0.0046	390 (55; –), 444 (56; 5.08); 0.032
Ir3	290 (5.17), 325 (5.07), 356 (4.90), 384 (4.67), 404 (4.72), 605 (3.04)	825 (380), 919 (–), 1035 (–), 1180 (–); 0.007	423 (392; –), 549 (405; –), 725 (380; –); –

[a] Electronic absorption band maxima (λ_{abs}) and molar extinction coefficients ($\log \epsilon$) in CH_2Cl_2 at room temperature. [b] Room temperature emission band maxima (λ_{em}) and lifetimes (τ_{em}) in CH_2Cl_2 ($c = 1 \times 10^{-5}$ mol/L). For emission quantum yields determination, $[\text{Ru}(\text{bpy})_3]\text{Cl}_2$ ($\Phi_{\text{em}} = 0.097$, $\lambda_{\text{ex}} = 436$ nm) in a degassed acetonitrile solution was used as the reference for **Ir1** and **Ir2**, while IRF140 ($\Phi_{\text{em}} = 0.167$, $\lambda_{\text{ex}} = 804$ nm) in a degassed ethanol solution was used as the reference for **Ir3**. [c] Nanosecond TA band maxima ($\lambda_{\text{T1-Tn}}$), triplet excited state lifetimes ($\tau_{\text{T1-Tn}}$) and quantum yields (Φ_{T}) measured in CH_3CN at room temperature.

To unambiguously understand the natures of the ground-state absorption, time-dependent density functional theory (TDDFT) calculations were carried out to simulate the absorption spectra and to obtain the natural transition orbitals (NTOs) corresponding to each optical transition in each complex. The simulated spectra for **Ir1–Ir3** are presented in Fig. 1(b) and the comparisons of the experimental and theoretical spectra are provided in ESI Fig. S1. Overall, the spectral features and the transition energies of the calculated spectra qualitatively agreed with the corresponding experimental spectra. As the NTOs in Tables 2 and S1 show, the low-energy absorption band(s) at >420 nm exclusively emanate from the ¹LLCT / ¹MLCT transitions. In view of the dark or extremely small oscillator strength of the S_1 and S_2 transitions in these complexes, the very weak absorption bands beyond 500 nm for **Ir1** and **Ir2**, and beyond 575 nm for **Ir3** could have contributions from the spin-forbidden ³ $\pi, \pi^*/³CT transitions that have been reported in many other Ir(III) complexes.^[14,26,34–36,41,46,47] The intense absorption bands at 320–420 nm (ESI Table S2) are dominated by the dppl ligand-localized ¹ π, π^* transitions, and mixed with some ¹MLCT/¹LLCT transitions. The NTOs in ESI Table S3 indicate that the short wavelength absorption bands at 280–320 nm predominantly arise from the dppl and N^N ligand localized spin-allowed ¹ π, π^* transitions, admixing with minor ¹MLCT/¹LLCT and intraligand charge transfer (¹ILCT) characters.$

Photoluminescence

To explore the triplet excited-state properties of **Ir1–Ir3**, the emission of these complexes was studied in different solvents at room temperature. The emission spectra and parameters in CH_2Cl_2 are provided in Fig. 2 and Table 1, and the spectra and parameters in other solvents are given in ESI Figure S3 and Table S4, respectively.

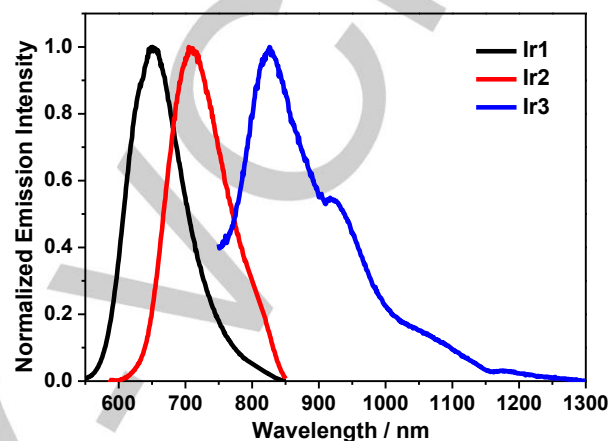


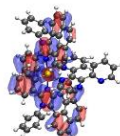
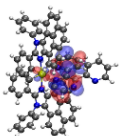
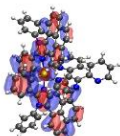
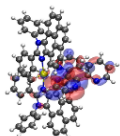
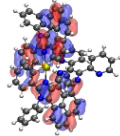
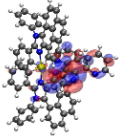
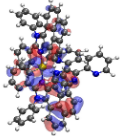
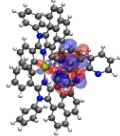
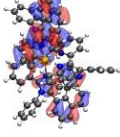
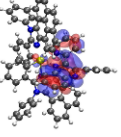
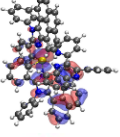
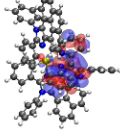
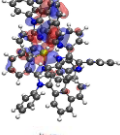
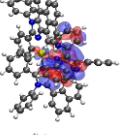
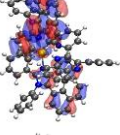
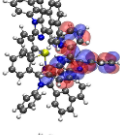
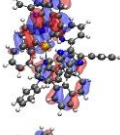
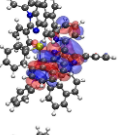

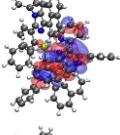
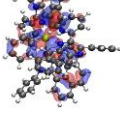
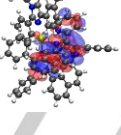
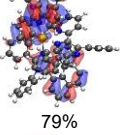
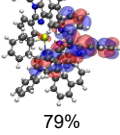
Fig. 2 Normalized emission spectra of **Ir1** ($\lambda_{\text{ex}} = 402$ nm), **Ir2** ($\lambda_{\text{ex}} = 403$ nm), and **Ir3** ($\lambda_{\text{ex}} = 404$ nm) in degassed CH_2Cl_2 solutions at room temperature.

The observed luminescence was sensitive to oxygen quenching, and the lifetimes were tens to hundreds of nanoseconds, indicating the phosphorescence nature of the emission. Going from **Ir1** to **Ir3**, the emission energy gradually decreased. Meanwhile, the spectral feature changed from featureless to structured, accompanied by a shortened lifetime from **Ir1** to **Ir2**, but an increased lifetime for **Ir3**. The lack of monotonic trend for the spectral feature and the emission lifetime is indicative of a different emitting state in **Ir3** from those in **Ir1** and **Ir2**. This notion was supported by the NTOs calculated by ΔSCF TDDFT.

As shown in Table 3, the electrons in the T_1 states were all localized on the N^N ligands and the d orbitals of Ir(III), while the holes were on the dppl ligands and a different d orbital of Ir(III) in **Ir1** and **Ir2**, but on the N^N and d orbital in **Ir3**. Therefore, the emitting states of **Ir1** and **Ir2** have the ³LLCT/³MLCT/³LMCT (ligand-to-metal charge transfer) configurations in nature; whereas the emitting state of **Ir3** is the N^N ligand-localized ³ π, π^* state. Because the electrons in all three complexes involved the N^N ligands, and the extended π -conjugation could stabilize the electrons, the reduced electron-hole gap decreased the emission energies going from **Ir1** to **Ir3**. Moreover, the charge transfer nature of the emitting states in **Ir1** and **Ir2** resulted in the shorter emission lifetime and lower emission quantum yield when the emission energy decreased from **Ir1** to **Ir2**. This trend is consistent with the energy gap law.^[48,49]

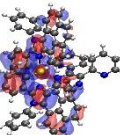
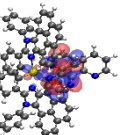
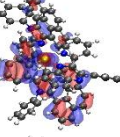
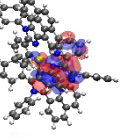
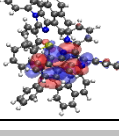
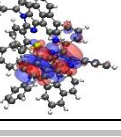
FULL PAPER

Table 2. Natural transition orbitals (NTOs) corresponding to the major transitions contributing to the low-energy absorption bands of **Ir1–Ir3** in CH₂Cl₂.

	States	Hole	Electron	States	Hole	Electron
Ir1	S ₁ 601 nm <i>f</i> = 0.003			S ₄ 438 nm <i>f</i> = 0.016		
	S ₆ 421 nm <i>f</i> = 0.014			S ₇ 420 nm <i>f</i> = 0.025		
Ir2^[a]	S ₂ 601 nm <i>f</i> = 0.002			S ₅ 445 nm <i>f</i> = 0.011		
	S ₆ 442 nm <i>f</i> = 0.014			S ₇ 434 nm <i>f</i> = 0.009		
Ir3^[a]	S ₂ 661 nm <i>f</i> = 0.002			S ₄ 503 nm <i>f</i> = 0.031		
	S ₆ 471 nm <i>f</i> = 0.010			S ₈ 428 nm <i>f</i> = 0.008		
					79%	79%
					20%	20%

[a] The S₁ state has zero oscillator strength, and its NTOs resemble those for the S₂ state. Thus, the NTOs for the S₁ state is not shown in this table. They are provided in ESI Table S1.

Table 3. NTOs representing the transitions contributing to the T₁ states of **Ir1–Ir3** in CH₂Cl₂ calculated by Δ SCF TDDFT method.

	T ₁ / nm	Hole	Electron
Ir1	794		
Ir2	860		
Ir3	1358		

Transient absorption (TA)

The RSA performance of a reverse saturable absorber is closely related to its excited-state absorption, triplet quantum yield, and triplet lifetime. Thus, the nanosecond transient difference absorption spectra of **Ir1–Ir3** were investigated in deoxygenated acetonitrile to further understand their triplet excited-state characteristics. The time-resolved TA spectra for **Ir1–Ir3** and the comparison of the TA spectra of these complexes immediately after laser excitation are presented in Fig. 3. The excited-state absorption parameters, *i.e.* the triplet excited-state lifetimes, extinction coefficients, and quantum yields, are compiled in Table 1. Because the TA lifetimes in CH₃CN are similar to the emission lifetimes measured in the same solution for **Ir1–Ir3**, the triplet excited states leading to the observed TA

FULL PAPER

can be attributed to the excited states state that emit, *i.e.* $^3\text{LLCT}/^3\text{MLCT}/^3\text{LMCT}$ states for **Ir1** and **Ir2**, and $^3\pi, \pi^*$ state for **Ir3**.

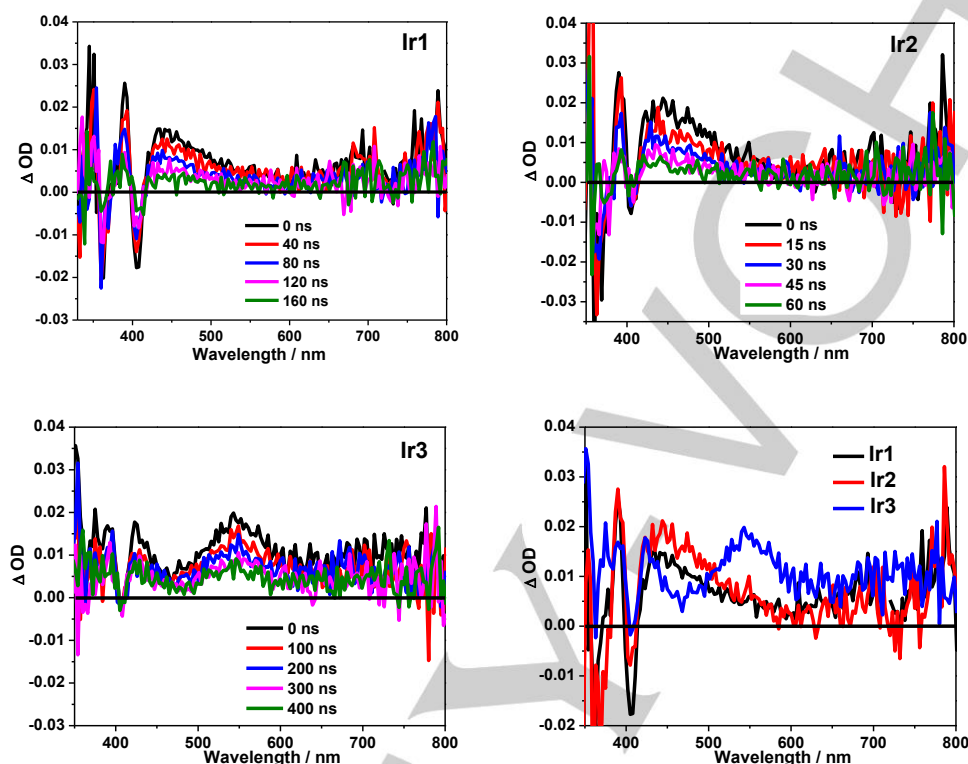


Fig. 3. Time-resolved nanosecond TA spectra of complexes **Ir1–Ir3** in deoxygenated acetonitrile solution, and the comparison of the TA spectra of **Ir1–Ir3** immediately after laser excitation. $A_{355} = 0.4$ in a 1 cm cuvette, $\lambda_{\text{ex}} = 355$ nm. (Note that the TA signals in the 700–800 nm region is noisy because the signals were weak in this region and it is close to the detector's detection limit. However, the band at ca. 702 nm in **Ir1** and at ca. 725 nm in **Ir3** is real.)

The TA spectra of **Ir1** and **Ir2** resembled each other, both with bleaching at ca. 360 nm and 405 nm, which are consistent with the UV–vis absorption band maxima in the same spectral regions; and positive absorption bands at 371–397 and 414–800 nm. The similar spectral feature reflected the similar configuration of their T_1 states. The positive absorption bands are similar to those observed in other Ir(III) complexes bearing the dppe ligands.^[21,24] Taking into account the fact that the T_1 state contains the $^3\text{LLCT}/^3\text{LMCT}$ characters, the observed positive absorption bands could be ascribed to the absorption from the dppe cation radical. In contrast, the TA spectrum of **Ir3** featured a broad positive absorption band in the 363–800 nm regions except for the very narrow and shallow bleaching bands centered at 370 and 405 nm. The TA spectrum of **Ir3** is similar to those observed from the other Ir(III) complex bearing the benzoquinoxaline motif in the C^N ligand.^[41,47] This feature along with the predominantly benzoquinoxaline localized $^3\pi, \pi^*$ nature of the T_1 state support the assignment that the observed TA of **Ir3** was indeed originated from the benzoquinoxaline-localized $^3\pi, \pi^*$ state.

Reverse saturable absorption

As the TA spectra in Fig. 3 displayed, complexes **Ir1–Ir3** all exhibited positive TA signals at 532 nm, implying a stronger triplet excited-state absorption at this wavelength than that of the ground state. Thus, RSA is anticipated to occur upon laser excitation at 532 nm. To ensure that identical number of complexes are excited to the singlet excited state, the concentration of each sample solution was adjusted to reach an 80% linear transmission in a 2 mm cuvette at 532 nm. At this condition, the observed difference in RSA should arise from the different characteristics of the triplet excited state. Using the 4.1 ns laser pulses, the nonlinear transmission experiment of **Ir1–Ir3** in acetonitrile was carried out and the results are provided in Fig. 4.

It is apparent that all complexes exhibited strong RSA, with the strength of RSA decreasing in the order of **Ir3** > **Ir1** ≥ **Ir2**. The RSA strength of **Ir1–Ir3** approximately paralleled the intensity of the TA signals immediately after laser pulse excitation at 532 nm (*i.e.* 0.005 for **Ir1** and **Ir2**, and 0.017 for **Ir3**). Although the ΔOD values are the same for **Ir1** and **Ir2**, a slightly stronger RSA was observed for **Ir1** because of its

FULL PAPER

slightly weaker ground-state absorption than that of **Ir2** (see the inset in Fig. 1). This is because the strength of RSA is mainly determined by the ratio of the excited-state absorption cross section (σ_{ex}) vs. that of the ground state (σ_0) at the same wavelength, a weaker ground-state absorption could increase the $\sigma_{\text{ex}}/\sigma_0$ ratio and thus enhance the RSA. For **Ir3**, the much stronger excited-state absorption at 532 nm compared to **Ir1** and **Ir2** accounted for its strongest RSA among these three complexes. Moreover, **Ir3** possesses the much broader ground-state absorption extending to 730 nm, a broader and stronger excited-state absorption in the visible spectral regions, and the longer triplet lifetime. These features could make it an attractive candidate as a broadband reverse saturable absorber, which will be studied in the near future.

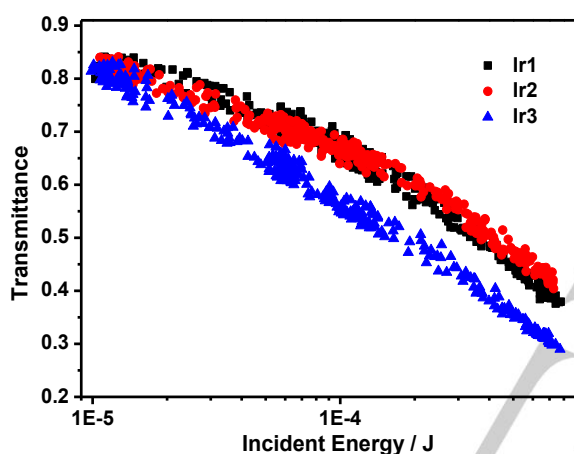


Fig. 4. Nonlinear transmission plots of **Ir1–Ir3** in acetonitrile at 532 nm with a linear transmittance of 80% in a 2-mm cuvette using the 4.1 ns laser pulses.

Conclusions

We have reported the synthesis, photophysics, and RSA of three cationic Ir(III) complexes with dppe as the C^N ligand and different 2,3-di(pyridine-2-yl)pyrazine derivatives as the N^N ligand. Spectroscopic methods and TDDFT calculations were used to understand the influence of π -conjugation of the N^N ligand on the UV-vis absorption and emission of the complexes. We found that increasing the π -conjugation of the N^N ligand caused a red-shift of the charge-transfer absorption bands in these complexes and increased the molar extinction coefficients of all of the absorption bands. Meanwhile, this structural variation switched the T_1 states from $^3\text{LLCT}/^3\text{MLCT}$ in **Ir1** and **Ir2** to the N^N ligand-localized $^3\pi, \pi^*$ state in **Ir3**, which not only red-shifted the emission spectrum of **Ir3**, but also prolonged the T_1 lifetime and drastically changed the transient absorption spectral features. The impact of the

π -conjugation on the ground-state and excited-state absorption consequently influenced the RSA of these complexes for ns laser pulses at 532 nm. The trend of the RSA strength, *i.e.* **Ir3** > **Ir1** \geq **Ir2**, is the result of the increased excited-state absorption and decreased ground-state absorption when the π -conjugation of the N^N ligand varied. The extended weak charge-transfer absorption band at 420 – 730 nm, along with the stronger triplet excited-state absorption in this spectral region promoted **Ir3** as a potential broadband reverse saturable absorber.

Experimental Section

Materials and synthesis

All chemicals and solvents were purchased from commercial sources and used as received without further purification. The ligands dppe (**L1**),^[50] 2,3-di(pyridine-2-yl)quinoxaline (**L2**),^[51] 2,3-di(pyridine-2-yl)benzo[*g*] quinoxaline (**L3**),^[52] dppe,^[25] and the Ir(III) dimer [Ir(dppe)₂Cl]₂,^[21] were prepared following the reported procedures. Column chromatography was carried out using silica gel (60 Å, 230–400 mesh) or Al₂O₃ gel (activated, neutral). The obtained complexes **Ir1–Ir3** were characterized by ¹H NMR, high-resolution electrospray ionization mass spectrometry (ESI-MS), and elemental analysis. The ¹H NMR spectra were measured on Bruker-400 spectrometer in CDCl₃ using tetramethylsilane (TMS) as the internal reference. High-resolution mass (HRMS) analyses were conducted on a Waters Synapt G2-Si mass spectrometer. Elemental analyses were performed by NuMega Resonance Laboratories, Inc. in San Diego, California.

General procedure for the synthesis of Ir1–Ir3

The [Ir(dppe)₂Cl]₂ dimer (61 mg, 0.03 mmol), corresponding N^N ligand (0.06 mmol), and AgSO₃CF₃ (15 mg, 0.06 mmol) were added in a mixed solvent (CH₂Cl₂:MeOH = 2:1 (v/v), 30 mL). The obtained mixture was degassed with N₂ for 30 min. and then heated to reflux for 24 h. After cooling to room temperature, NH₄PF₆ (49 mg, 0.3 mmol) was added and stirred for another 2 h. Solvent was then removed in vacuum. The residue was separated by column chromatography on alumina gel, eluting with CH₂Cl₂/hexanes (3:1 to 1:0 (v/v)) to afford the target complex.

Ir1. A red powder was obtained as the product (46 mg, 52%). ¹H NMR (400 MHz, CDCl₃): δ 8.86 (d, *J* = 2.9 Hz, 1H), 8.69 (d, *J* = 4.9 Hz, 1H), 8.59 (d, *J* = 2.9 Hz, 1H), 8.45 – 8.38 (m, 2H), 8.12 (q, *J* = 7.8 Hz, 1H), 8.09 – 7.85 (m, 18H), 7.85 – 7.78 (m, 1H), 7.73 – 7.63 (m, 2H), 7.59 (t, *J* = 7.9 Hz, 1H), 7.45 – 7.36 (m, 2H), 7.34 (d, *J* = 8.1 Hz, 1H), 7.32 – 7.27 (m, 2H), 7.21 (dd, *J* = 10.5, 3.2 Hz, 1H), 7.10 (td, *J* = 7.7, 1.7 Hz, 1H), 7.06 – 6.99 (m, 1H), 6.93 – 6.81 (m, 4H), 6.74 – 6.67 (m, 1H), 6.63 (dt, *J* = 5.0, 3.1 Hz, 1H), 6.47 (d, *J* = 8.1 Hz, 1H), 5.58 (d, *J* = 7.7 Hz, 1H). ESI-HRMS (*m/z*): calcd. for

FULL PAPER

$[\text{C}_{72}\text{H}_{44}\text{N}_8\text{Ir}]^+$, 1213.3325; found, 1213.3322. Anal. Calcd for $\text{C}_{72}\text{H}_{44}\text{F}_6\text{IrN}_8\text{P}\cdot 6\text{H}_2\text{O}$: C, 58.97; H, 3.85; N, 7.64. Found: C, 59.25; H, 3.97; N, 7.70.

Ir2. A brownish powder was obtained as the product (47 mg, 54%). ^1H NMR (400 MHz, CDCl_3): δ 8.69 (d, J = 6.7 Hz, 2H), 8.41 (d, J = 7.1 Hz, 1H), 8.24 (d, J = 7.2 Hz, 1H), 8.20 – 8.08 (m, 4H), 8.08 – 7.78 (m, 12H), 7.79 – 7.64 (m, 4H), 7.64 – 7.58 (m, 1H), 7.55 (t, J = 7.9 Hz, 1H), 7.45 (d, J = 7.4 Hz, 1H), 7.39 – 7.29 (m, 4H), 7.25 – 7.15 (m, 2H), 7.09 (dd, J = 6.5, 4.9 Hz, 1H), 7.02 (td, J = 7.7, 0.5 Hz, 2H), 6.83 (ddd, J = 11.1, 9.0, 4.4 Hz, 4H), 6.78 – 6.72 (m, 1H), 6.71 – 6.66 (m, 1H), 6.34 (t, J = 7.8 Hz, 2H), 6.29 (d, J = 7.1 Hz, 1H), 5.67 (d, J = 7.8 Hz, 1H). ESI–HRMS (m/z): calcd. for $[\text{C}_{76}\text{H}_{46}\text{N}_8\text{Ir}]^+$, 1263.3481; found, 1263.3477. Anal. Calcd for $\text{C}_{76}\text{H}_{46}\text{F}_6\text{IrN}_8\text{P}\cdot 3\text{H}_2\text{O}$: C, 63.19; H, 3.49; N, 7.76. Found: C, 62.99; H, 3.72; N, 7.40.

Ir3. A brownish powder was obtained as the product (34 mg, 39%). ^1H NMR (CDCl_3 , 400 MHz): δ 9.15 – 9.04 (m, 1H), 8.80 – 8.67 (m, 2H), 8.59 (s, 1H), 8.50 – 8.35 (m, 1H), 8.22 (d, J = 8.5 Hz, 1H), 8.17 – 7.88 (m, 12H), 7.89 – 7.61 (m, 7H), 7.60 – 7.51 (m, 3H), 7.49 – 7.38 (m, 2H), 7.33 (t, J = 7.8 Hz, 1H), 7.25 – 7.16 (m, 3H), 7.16 – 7.07 (m, 2H), 7.05 – 6.92 (m, 2H), 6.92 – 6.74 (m, 5H), 6.70 (dd, J = 8.0, 1.3 Hz, 1H), 6.20 (dd, J = 7.9, 0.9 Hz, 1H), 6.11 (t, J = 7.8 Hz, 1H), 5.39 (d, J = 7.7 Hz, 1H), 5.24 (d, J = 8.0 Hz, 1H). ESI–HRMS (m/z): calcd. for $[\text{C}_{80}\text{H}_{48}\text{N}_8\text{Ir}]^+$, 1313.3639; found, 1313.3652. Anal. Calcd for $\text{C}_{80}\text{H}_{48}\text{F}_6\text{IrN}_8\text{P}\cdot 0.7\text{CH}_2\text{Cl}_2$: C, 62.50; H, 3.26; N, 7.18. Found: C, 62.37; H, 3.41; N, 7.19.

Photophysical and nonlinear transmission measurements

The UV–vis absorption spectra of **Ir1–Ir3** were recorded on a Varian Cary 50 spectrophotometer. The emission spectra of **Ir1** and **Ir2** were recorded on a HORIBA FluoroMax–4 fluorometer/phosphorometer. A PTI Quantamaster equipped with a Hamamatsu R5509–42 near-infrared PMT was used to record the NIR emission spectrum of **Ir3** in CH_2Cl_2 . The emission quantum yields were obtained in deaerated solutions using relative actinometry method,^[53] with $[\text{Ru}(\text{bpy})_3]\text{Cl}_2$ (Φ_{em} = 0.097 in degassed acetonitrile solution, λ_{ex} = 436 nm)^[54] being used as the reference for **Ir1** and **Ir2**, and IR-140 (5,5'-dichloro-11-diphenylamino-3,3'-diethyl-10,12-ethylenethiatricarbocyanine perchlorate, Φ_{em} = 0.167 in degassed ethanol solution, λ_{ex} = 804 nm)^[55] for **Ir3**. The nanosecond transient difference absorption (TA) spectra of **Ir1–Ir3** were measured on an Edinburgh LP920 laser flash photolysis spectrometer in acetonitrile solutions. The third-harmonic output (355 nm) of a Nd:YAG laser (Quantel Brilliant, 4.1 ns, the repetition rate was set to 1 Hz) was used as the excitation source. Each sample solution was degassed with nitrogen for 40 min. before the measurement. By using the singlet depletion method,^[56] the triplet excited-state molar extinction coefficients (ϵ_T) of **Ir1–Ir3** at the TA band maxima were determined. The triplet

excited-state quantum yields were then obtained using the relative actinometry method,^[57] with the benzene solution of SiNc (ϵ_{590} = 70,000 $\text{M}^{-1} \text{cm}^{-1}$, Φ_T = 0.20)^[58] being used as the reference. The setup and details of the nonlinear transmission measurement were the same as those reported earlier by our group.^[34,59]

Computational methodology

The ground and excited-state properties of complexes **Ir1–Ir3** were simulated using density functional theory (DFT) and linear response time-dependent DFT (TDDFT) calculations. Gaussian09^[60] was used to compute the ground and excited state properties of complexes applying the B3LYP^[61] functional and the mixed basis set (LANL2DZ for Ir,^[62] and 6-31G* for H, C, and N^[63]). The effect of dichloromethane solvent was implicitly included through the Conductor Polarized Continuum Model (CPCM).^[64,65]

The chosen DFT-based methodology represents one of the currently most popular density functionals and basis sets, which previously has shown good agreement with UV-Vis experimental data for various Pt(II), Ru(II) and Ir(III) complexes.^[33–42] The validity of various hybrid DFT functionals with different portions of Hartree–Fock (HF) exchange has been widely tested for description of geometries and optical properties of various transition metal complexes.^[66,67] It has been shown that B3LYP functional with 20% of HF provided substantial agreement with the experimental absorption spectra for octahedral Ru(II)^[68] and Ir(III) complexes.^[69] While changes in the HF portion typically resulted in a uniform shift of the spectral energies, the qualitative spectral features and the nature of optical transitions were insignificantly affected.

Employing an effective core potentials (ECPs) basis such as LANL2DZ for transition metals and using all-electron basis sets for all other non-transition-metal atoms have become a common practice in computing transition metal containing systems.^[70] ECPs are parameterized to implicitly account for scalar relativistic effects via two-electron spin-orbit coupling (SOC) integrals implemented to an effective one-electron operator for the elements across the periodic table as an effective nuclear charge.^[71] In our previous work,^[36] we compared the effect of SOC on optical spectra of cationic Ir(III) complexes bearing 2-(2-quinolinyl)quinoxaline ligands by directly applying relativistic TDDFT using the ZORA Hamiltonian.^[72] These calculations demonstrated that absorption spectra calculated by TDDFT and TDDFT-ZORA closely agree with each other and with the experimental absorption spectra, suggesting a minor effect of explicit implementation of SOC to the TDDFT calculations. Therefore, an explicit account for SOC was avoided in the current calculations to save computational time.

The oscillator strengths and excitation energies obtained from TDDFT calculations were used to simulate the

FULL PAPER

absorption spectra of **Ir1–Ir3** using Gaussian broadening with a line-width of 0.08 eV to reproduce the inhomogeneous thermal broadening of the experimental spectra, following the procedure in Ref. [73]. The emission energies of **Ir1–Ir3** were obtained using the Δ SCF approach based on TDDFT. With this method, we computed the phosphorescence energy using the triplet equilibrium geometry for calculating the optical transition between the singlet ground state (S_0) and the lowest triplet excited state (T_1).^[21] The nature of the singlet absorption ($S_0 \rightarrow S_n$) and the triplet emission ($T_1 \rightarrow S_0$) was demonstrated by computing the natural transition orbitals (NTOs)^[74] for relevant optical transitions. The NTOs were visualized using VMD^[75] with an isosurface of 0.02.

Acknowledgments

The experimental part of this work was supported by the National Science Foundation grant DMR-1411086. The computational simulation part of the work was supported by the National Science Foundation grant CHE-1800476. S.K. thanks the Center for Computationally Assisted Science and Technology (CCAST) at North Dakota State University for computational resources and administrative support.

Keywords: Ir(III) complexes • photophysics • red absorption • near-IR emission • reverse saturable absorption

- [1] I. M. Dixon, J.-P. Collin, J.-P. Sauvage, L. Flamigni, S. Encinas, F. Barigelletti, *Chem. Soc. Rev.* **2000**, 29, 385–391.
- [2] J. I. Goldsmith, W. R. Hudson, M. S. Lowry, T. H. Anderson, S. Bernhard, *J. Am. Chem. Soc.* **2005**, 127, 7502–7510.
- [3] S. Lamansky, P. Djurovich, D. Murphy, F. Abdel-Razzaq, R. Kwong, I. Tsyba, M. Bortz, B. Mui, R. Bau, M. E. Thompson, *Inorg. Chem.* **2001**, 40, 1704–1711.
- [4] E. Holder, B. M. W. Langeveld, U. S. Schubert, *Adv. Mater.* **2005**, 17, 1109–1121.
- [5] P.-T. Chou, Y. Chi, *Chem. –Eur. J.* **2007**, 13, 380–395.
- [6] W.-Y. Wong, C.-L. Ho, *J. Mater. Chem.* **2009**, 19, 4457–4482.
- [7] J. Sun, F. Zhong, X. Yi, J. Zhao, *Inorg. Chem.* **2013**, 52, 6299–6310.
- [8] L. Ma, S. Guo, J. Sun, C. Zhang, J. Zhao, H. Guo, *Dalton Trans.* **2013**, 42, 6478–6488.
- [9] Q. Zhao, M. Yu, L. Shi, S. Liu, C. Li, M. Shi, Z. Zhou, C. Huang, F. Li, *Organometallics* **2010**, 29, 1085–1091.
- [10] J. Liu, Y. Liu, Q. Liu, C. Li, L. Sun, F. Li, *J. Am. Chem. Soc.* **2011**, 133, 15276–15279.
- [11] N. D. McDaniel, F. J. Coughlin, L. L. Tinker, S. Bernhard, *J. Am. Chem. Soc.* **2008**, 130, 210–217.
- [12] J. D. Blakemore, N. D. Schley, D. Balcells, J. F. Hull, G. W. Olack, C. D. Incavito, O. Eisenstein, G. W. Brudvig, R. H. Crabtree, *J. Am. Chem. Soc.* **2010**, 132, 16017–16029.
- [13] B. Liu, S. Monro, L. Lystrom, C. G. Cameron, K. Colón, H. Yin, S. Kilina, S. A. McFarland, W. Sun, *Inorg. Chem.* **2018**, 57, 9859–9872.
- [14] C. Wang, L. Lystrom, H. Yin, M. Hetu, S. Kilina, S. A. McFarland, W. Sun, *Dalton Trans.* **2016**, 45, 16366–16378.
- [15] L. He, Y. Li, C.-P. Tan, R.-R. Ye, M.-H. Chen, J.-J. Cao, L.-N. Ji, Z.-W. Mao, *Chem. Sci.* **2015**, 6, 5409–5418.
- [16] Y. Li, N. Dandu, R. Liu, S. Kilina, W. Sun, *Dalton Trans.* **2014**, 43, 1724–1735.
- [17] Y. Li, N. Dandu, R. Liu, Z. Li, S. Kilina, W. Sun, *J. Phys. Chem. C* **2014**, 118, 6372–6384.
- [18] R. D. Costa, E. Ortí, H. J. Bolink, F. Monti, G. Accorsi, N. Armaroli, *Angew. Chem., Int. Ed.* **2012**, 51, 8178–8211.
- [19] I. Romanenko, D. Gajan, R. Sayah, D. Crozet, E. Jeanneau, C. Lucas, L. Leroux, L. Veyre, A. Lesage, L. Emsley, E. Lacôte, C. Thieuleux, *Angew. Chem., Int. Ed.* **2015**, 127, 13129–13133.
- [20] M. Schulze, A. Steffen, F. Würthner, *Angew. Chem., Int. Ed.* **2015**, 54, 1570–1573.
- [21] B. Liu, L. Lystrom, S. Kilina, W. Sun, *Inorg. Chem.* **2017**, 56, 5361–5370.
- [22] X. Zeng, M. Tavasli, I. F. Perepichka, A. S. Batsanov, M. R. Bryce, C.-J. Chiang, C. Rothe, A. P. Monkman, *Chem. –Eur. J.* **2008**, 14, 933–943.
- [23] K.-Y. Kim, R. T. Farley, K. S. Schanze, *J. Phys. Chem. B* **2006**, 110, 17302–17304.
- [24] Z. Li, P. Cui, C. Wang, S. Kilina, W. Sun, *J. Phys. Chem. C* **2014**, 118, 28764–28775.
- [25] X. Yi, P. Yang, D. Huang, J. Zhao, *Dyes Pigm.* **2013**, 96, 104–115.
- [26] Q. Zhao, S. Liu, M. Shi, C. Wang, M. Yu, L. Li, F. Li, T. Yi, C. Huang, *Inorg. Chem.* **2006**, 45, 6152–6160.
- [27] C. Li, L. Zhang, R. Wang, Y. Song, Y. Wang, *J. Opt. Soc. Am. B* **1994**, 11, 1356–1360.
- [28] J. W. Perry, K. Mansour, S. R. Marder, K. J. Perry, D. Alvarez, I. Choong, *Opt. Lett.* **2005**, 19, 625–627.
- [29] A. Penzkofer, *Appl. Phys. B* **1988**, 46, 43–60.
- [30] K. Reddy, *Curr. Sci.* **1991**, 61, 520–526.
- [31] S. Speiser, M. Orenstein, *Appl. Opt.* **1988**, 27, 2944–2948.
- [32] Y. B. Band, D. Harter, R. Bavli, *Chem. Phys. Lett.* **1986**, 126, 280–284.
- [33] Y. Li, N. Dandu, R. Liu, L. Hu, S. Kilina, W. Sun, *ACS Appl. Mater. Interfaces* **2013**, 5, 6556–6570.
- [34] B. Liu, L. Lystrom, S. Kilina, W. Sun, *Inorg. Chem.* **2019**, 58, 476–488.
- [35] R. Liu, N. Dandu, J. Chen, Y. Li, Z. Li, S. Liu, C. Wang, S. Kilina, B. Kohler, W. Sun, *J. Phys. Chem. C* **2014**, 118, 23233–23246.
- [36] W. Sun, C. Pei, T. Lu, P. Cui, Z. Li, C. McCleese, Y. Fang, S. Kilina, Y. Song, C. Burda, *J. Mater. Chem. C* **2016**, 4, 5059–5072.
- [37] C. Pei, P. Cui, C. McCleese, S. Kilina, C. Burda, W. Sun, *Dalton Trans.* **2015**, 44, 2176–2190.
- [38] X. Zhu, L. Lystrom, S. Kilina, W. Sun, *Inorg. Chem.* **2016**, 55, 11908–11919.
- [39] Z. Li, H. Li, B. J. Gifford, W. D. N. Peiris, S. Kilina, W. Sun, *RSC Adv.* **2016**, 6, 41214–41228.
- [40] X. Zhu, P. Cui, S. Kilina, W. Sun, *Inorg. Chem.* **2017**, 56, 13715–13731.
- [41] L. Wang, P. Cui, S. Kilina, W. Sun, *J. Phys. Chem. C* **2017**, 121, 5719–5730.
- [42] R. Liu, N. Dandu, C. McCleese, Y. Li, T. Lu, H. Li, D. Yost, C. Wang, S. Kilina, C. Burda, W. Sun, *Eur. J. Inorg. Chem.* **2015**, 31, 5241–5253.
- [43] T. M. Pritchett, M. J. Ferry, W. M. Shensky III, A. G. Mott, D. J. Stewart, S. L. Long, J. E. Haley, Z. Li, W. Sun, *Opt. Lett.* **2015**, 40, 186–189.
- [44] T. M. Pritchett, M. J. Ferry, A. G. Mott, W. Shensky III, J. E. Haley, R. Liu, W. Sun, *Opt. Mater.* **2015**, 39, 195–198.
- [45] H. Zhao, P. V. Simpson, A. Barlow, G. J. Moxey, M. Morshedi, N. Roy, R. Philip, C. Zhang, M. P. Cifuentes, M. G. Humphrey, *Chem. Eur. J.* **2015**, 21, 11843–11854.
- [46] S.-H. Wu, J.-W. Ling, S.-H. Lai, M.-J. Huang, C. H. Cheng, I.-C. Chen, *J. Phys. Chem. A* **2010**, 114, 10339–10344.
- [47] L. Wang, H. Yin, P. Cui, M. Hetu, C. Wang, S. Monro, R. D. Schaller, C. G. Cameron, B. Liu, S. Kilina, S. A. McFarland, W. Sun, *Dalton Trans.* **2017**, 46, 8091–8103.
- [48] J. V. Caspar, E. M. Kober, B. P. Sullivan, T. J. Meyer, *J. Am. Chem. Soc.* **1982**, 104, 630–632.
- [49] J. V. Caspar, T. J. Meyer, *J. Phys. Chem.* **1983**, 87, 952–957.
- [50] I. L. Karle, Y. B. R. D. Rajesh, S. Ranganathan, *J. Chem. Cryst.* **2005**, 35, 835–845.

FULL PAPER

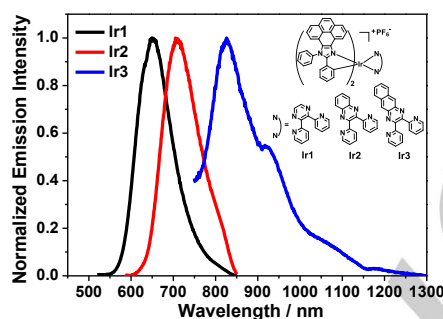
- [51] A. Ohta, S. Masano, S. Iwakura, A. Tamura, H. Watahiki, M. Tsutsui, Y. Akita and T. Watanabe, *J. Heterocycl. Chem.* **1982**, *19*, 465–472.
- [52] R. Bellam, D. Jaganyi, A. Mambanda, R. Robinson, *New J. Chem.* **2018**, *42*, 12557–12569.
- [53] J. N. Demas, G. A. Crosby, *J. Phys. Chem.* **1971**, *75*, 991–1024.
- [54] K. Rurack, M. Spieles, *Anal. Chem.* **2011**, *83*, 1232–1242.
- [55] K. Suzuki, A. Kobayashi, S. Kaneko, K. Takehira, T. Yoshihara, H. Ishida, Y. Shiina, S. Oishi, S. Tobita, *Phys. Chem. Chem. Phys.* **2009**, *11*, 9850–9860.
- [56] I. Carmichael, G. L. Hug, *J. Phys. Chem. Ref. Data* **1986**, *15*, 1–250.
- [57] C. V. Kumar, L. Qin, P. K. Das, *J. Chem. Soc., Faraday Trans. 2* **1984**, *80*, 783–793.
- [58] P. A. Firey, W. E. Ford, J. R. Sounik, M. E. Kenney, M. A. J. Rodgers, *J. Am. Chem. Soc.* **1988**, *110*, 7626–7630.
- [59] F. Guo, W. Sun, Y. Liu, K. Schanze, *Inorg. Chem.* **2005**, *44*, 4055–4065.
- [60] M. J. Frisch, G. W. Trucks, H. B. Schlegel, G. E. Scuseria, M. A. Robb, J. R. Cheeseman, G. Scalmani, V. Barone, B. Mennucci, G. A. Petersson, H. Nakatsuji, M. Caricato, X. Li, H. P. Hratchian, A. F. Izmaylov, J. Bloino, G. Zheng, J. L. Sonnenberg, M. Hada, M. Ehara, K. Toyota, R. Fukuda, J. Hasegawa, M. Ishida, T. Nakajima, Y. Honda, O. Kitao, H. Nakai, T. Vreven, J. A. Montgomery Jr., J. E. Peralta, F. Ogliaro, M. Bearpark, J. J. Heyd, E. Brothers, K. N. Kudin, V. N. Staroverov, R. Kobayashi, J. Normand, K. Raghavachari, A. Rendell, J. C. Burant, S. S. Iyengar, J. Tomasi, M. Cossi, N. Rega, J. M. Millam, M. Klene, J. E. Knox, J. B. Cross, V. Bakken, C. Adamo, J. Jaramillo, R. Gomperts, R. E. Stratmann, O. Yazyev, A. J. Austin, R. Cammi, C. Pomelli, J. W. Ochterski, R. L. Martin, K. Morokuma, V. G. Zakrzewski, G. A. Voth, P. Salvador, J. J. Dannenberg, S. Dapprich, A. D. Daniels, Ö. Farkas, J. B. Foresman, J. V. Ortiz, J. Cioslowski and D. J. Fox, Gaussian09, Revision A.1, Gaussian Inc., Wallingford CT, **2009**.
- [61] C. Lee, W. Yang, R. G. Parr, *Phys. Rev. B: Condens. Matter* **1988**, *37*, 785–789.
- [62] P. J. Hay, W. R. Wadt, *J. Chem. Phys.* **1985**, *82*, 270–283.
- [63] C. Adamo, V. Barone, *J. Chem. Phys.* **1999**, *110*, 6158–6170.
- [64] V. Barone, M. Cossi, J. Tomasi, *J. Comput. Chem.* **1998**, *19*, 404–417.
- [65] M. Cossi, V. Barone, R. Cammi, J. Tomasi, *Chem. Phys. Lett.* **1996**, *255*, 327–335.
- [66] C. J. Cramer, D. G. Truhlar, *Phys. Chem. Chem. Phys.* **2009**, *11*, 10757–10816.
- [67] C. Garino, L. Salassa, *Phil. Trans. R. Soc. A* **2013**, *371*, 20120134.
- [68] E. Badaeva, V. V. Albert, S. Kilina, A. Koposov, M. Sykorad S. Tretiak, *Phys. Chem. Chem. Phys.* **2010**, *12*, 8902–8913.
- [69] J.-P. Zhang, Y. Wang, J.-B. Ma, L. Jin, F.-T. Liu, F.-Q. Bai, *RSC Adv.* **2018**, *8*, 19437–19448.
- [70] Y. Yang, M. N. Weaver, K. M. Merz Jr, *J. Phys. Chem. A* **2009**, *113*, 9843–9851.
- [71] S. Koseki, M. S. Gordon, M. W. Schmidt, N. Matsunaga, *J. Phys. Chem.* **1995**, *99*, 12764–12772.
- [72] E. van Lenthe, E.-J. Baerends, J. G. Snijders, *J. Chem. Phys.* **1994**, *101*, 9783–9792.
- [73] J. A. Bjorgaard, A. E. Sifain, T. Nelson, T. W. Myers, J. M. Veauthier, D. E. Chavez, R. J. Scharff, S. Tretiak, *J. Phys. Chem. A* **2016**, *120*, 4455–4464.
- [74] R. L. Martin, *J. Chem. Phys.* **2003**, *118*, 4775–4777.
- [75] W. Humphrey, A. Dalke, K. Schulten, *J. Mol. Graph.* **1996**, *14*, 33–38.

FULL PAPER

Entry for the Table of Contents

FULL PAPER

Extending the π -conjugation of the 2,3-di(pyridin-2-yl)pyrazine ligand in monocationic Ir(III) complexes red-shifted the charge transfer absorption bands to far-red and the phosphorescence to the near-IR regions. This structural modification also made the complexes better broadband reverse saturable absorbers.

**Ir(III) Complexes**

Bingqing Liu, Levi Lystrom, Colin G. Cameron, Svetlana Kilina, Sherri A. McFarland, and Wenfang Sun*

Page 1 – Page 8

Monocationic Iridium(III) Complexes with Far-Red Charge Transfer Absorption and Near-IR Emission: Synthesis, Photophysics, and Reverse Saturable Absorption